of the cryoscopy apparatus, and P. Gregory for some MNDO calculations. Financial support from the Deutsche Forschungsgemeinschaft, the Fonds der Chemischen Industrie, and the Convex Computer Corp. is gratefully acknowledged. M.R.S. would like to thank the U.S. Department of Education for a National Needs Fellowship.

Note Added in Proof. Since submission of this manuscript, a number of papers pertinent to the title compounds have been published. Andersen et al.[63] described the crystal structure of $[Li(TMEDA)_2][Li_2(TMEDA)_2\text{-}\mu\text{-}n^5,n^5\text{-}MeC_5H_4][n^5\text{-}MeC_5H_4)_6U_2(\mu\text{-}Me)]_2$. Therein, the linear Li–MeCp–Li cation can be thought of as an inverse of sandwich **6**. Farona et al.[64] analyzed the iron derivative of isodiCp and its dehydro isomer **46** by means of two-dimensional NMR. All possible exo/exo, exo/endo, and endo/endo isomers of both species were studied. The same group also describes 2D NMR studies of the analogous Ti and Zr derivatives.[65] Brandsma et al. determined the degree of aggregation of CpLi in liquid ammonia by means of cryoscopy.[66] A monomer–dimer equilibrium (60:40) was detected. This agrees favorably with our NMR findings described above. Köhler et al.[67] recorded the ^{13}C NMR spectra of lithium and potassium bicyclo[3.2.1]octa-2,6-dienide. Whereas the potassium compound is a CIP, a CIP–SSIP equilibrium was detected for the lithium compound, very similar to our findings described in this paper.

UV Resonance Raman Saturation Spectroscopy Measures Protein Aromatic Amino Acid Excited State Relaxation Rates

Paul A. Harmon, Junji Teraoka,† and Sanford A. Asher*

Contribution from the Department of Chemistry, University of Pittsburgh, Pittsburgh, Pennsylvania 15260. *Received February 16, 1990*

Abstract: We demonstrate the utility of the new technique of UV resonance Raman saturation spectroscopy (Teraoka et al. *J. Am. Chem. Soc.* **1990**, *112*, 2892) for studying tryptophan and tyrosine excited-state relaxation rates in proteins. This technique monitors the ground-state population during UV pulsed laser excitation. It reports on ground-state recovery rates for aromatic amino acid residues which depend upon energy-transfer processes and photoionization quantum yields. We demonstrate the dependence of the relaxation rates on aromatic amino acid environment in lysozyme, myoglobin, and glucagon and examine energy transfer between aromatic amino acid residues in a tryptophan–tyrosine dimer. In contrast to aromatic amino acid solution studies, we find little photoionization in the proteins studied. This technique is of general utility for studying relaxation rates of chromophores, even those with weak fluorescence such as phenylalanine and tyrosine in proteins containing tryptophan residues. We discuss the utility of this technique for future biological and chemical applications. We also demonstrate the dependence of the aromatic amino acid residue Raman cross sections to the protein residue environment.

Introduction

The establishment of molecular structure and function relationships in biomolecules is hindered by the size and complexity of these systems. A host of techniques has been developed and applied to examine different facets of molecular structure and dynamics for these macromolecules.[1,2] For example, X-ray diffraction, NMR, CD, and numerous other spectroscopies have been applied to studying various aspects of protein structure in order to define enzymatic mechanisms at the molecular level. An incisive glimpse into the enzymatic mechanism generally results only from combining the information derived from each separate approach. Thus, the development of new techniques for studying biomolecular structure is crucial for progress in biochemistry and biophysics; as more information is obtained, more detailed molecular questions can be posed.

A number of powerful optical spectroscopic techniques have focused on the UV spectral region,[3] such as UV absorption spectroscopy, fluorescence spectroscopy, and UV CD spectroscopy. Absorption techniques have concentrated on studying aromatic amino acid residues such as tryptophan (TRP), tyrosine (TYR), and phenylalanine (PHE) in proteins, while fluorescence studies of proteins have been limited primarily to TRP residues.[4-8] The importance of these results derives from the valuable information obtained on the protein structure by probing the aromatic amino acid environments. The power of TRP residue fluorescence lifetime measurements, for example, rests on the exquisite sensitivity of excited-state relaxation rates to the immediate fluorophore environment. UV resonance Raman spectroscopy (UVRR) has recently shown the ability to selectively examine the vibrational spectra of all three aromatic amino acids in proteins.[9-11] The utility of UVRR is based on the wavelength dependence of the resonance effect and the dependence of the Raman vibrational frequencies on the residue environment.[9-13] In addition, we recently demonstrated a new technique, UVRR saturation spectroscopy,[14] that uses UVRR intensities to monitor the aromatic amino acid relaxation rates back to the ground state. This previous

* Author to whom correspondence should be addressed.
† Present address: Osaka City University, Osaka, Japan.

(1) See, for example: Biophysics; Hoppe, W., Lohmann, W., Markl, H., Ziegler, H. Eds.; Springer-Verlag: Heidelberg, 1983.
(2) Cantor, C. R.; Schimmel, P. R. Biophysical Chemistry; Bartlett, A. C., Vapnek, P. C., McCombs, L. W., Eds.; W. H. Freeman and Co.: 1980; Vol. II.
(3) Demchenko, A. P. Ultraviolet Spectroscopy of Proteins; Springer-Verlag: Berlin, 1986.
(4) Beechem, J. M.; Brand, L. *Ann. Rev. Biochem.* **1985**, *54*, 43.
(5) Longworth, J. W. In *Time Resolved Fluorescence Spectroscopy in Biochemistry and Biology*; Cundall, R. B., Dale, R. E. Eds.; Plenum: London, 1983; p 651.
(6) Lakowicz, J. R. In *Principles of Fluorescence Spectroscopy*; Plenum: New York, 1983.
(7) Petrich, J. W.; Longworth, J. W.; Fleming, G. R. *Biochemistry* **1987**, *26*, 2711.
(8) Hutnik, C. M.; Szabo, A. G. *Biochemistry* **1989**, *28*, 3923, 3935.
(9) Asher, S. A. *Ann. Rev. Phys. Chem.* **1988**, *39*, 537.
(10) Harada, I.; Takeuchi, H. In *Spectroscopy of Biological Systems*; Clark, R. J. H., Hestor, R. E., Eds.; John Wiley and Sons: 1986; Chapter 3.
(11) Spiro, T. G.; Grygon, C. A. *J. Mol. Struct.* **1988**, *173*, 79.
(12) Su, C.; Park, Y. D.; Lui, G.-Y.; Spiro, T. G. *J. Am. Chem. Soc.* **1989**, *111*, 3457.
(13) Kaminiaka, S.; Ogura, T.; Kitagawa, T. *J. Am. Chem. Soc.* **1990**, *112*, 23.

0002-7863/90/1512-8789$02.50/0

UVRR saturation study of simple TRP derivatives showed quantitative agreement between ground-state recovery rates and time-resolved fluorescence measurements of the TRP derivative fluorescent excited-state lifetimes.

We report here an extension of UVRR saturation spectroscopy to examine aromatic amino acid residue excited-state relaxation rates in proteins. We find the Raman saturation methodology can readily monitor the sensitivity of the aromatic residues excited-state relaxation rates to protein environment. The saturation methodology involves careful monitoring of the laser power dependence of the aromatic amino acid UVRR intensities. The ground state is depopulated during the laser pulse via optical absorption as excited states are populated. This depopulation process competes with ground-state repopulation, which derives from excited-state relaxation processes. This competition gives rise to characteristic nonlinear changes in the Raman intensity of ground-state species as the number of photons per incident excitation pulse is varied. The degree of nonlinearity observed can then be related to the rate at which the excited states relax. This method of examining chromophore relaxation rates in proteins has the advantages of the selectivity and the vibrational resolution inherent in resonance Raman scattering, and it does not require chromophores which strongly fluoresce. The determination of the excited-state relaxation rate of a given chromophore requires only a single resolved vibrational band. This selectivity is particularly poignant in protein studies where other ground-state recovery techniques, such as the laser power dependence of the absorbance, are likely to be hopelessly complicated by the absorption spectral overlap of TRP, TYR, PHE, amide bands, and other protein chromophores.

We examine initially as a model system a TRP–TYR dimer and find that the ground-state recovery rates derived from the Raman saturation methodology clearly reflect interresidue excited-state quenching interactions. We then apply this Raman saturation methodology to the TRP and TYR residues in myoglobin, lysozyme, and glucagon. The same interresidue interactions which control the TRP residue fluorescence behavior are found to dominate TRP ground-state recovery processes. TYR residue excited-state relaxation rates in these proteins are measured for the first time. We also study the photoionization quantum yields from TRP and TYR higher excited singlet states. The quantitative resonance Raman cross sections derived from these studies differ for TYR and TRP residues between the different proteins. We discuss the utility of monitoring TRP, TYR, and PHE excited-state relaxations for probing protein conformational dynamics.

Experimental Section

N-Acetyl-L-tryptophanamide (NATRPAM), L-tryptophanamide (TRPAM), *N*-acetyl-L-tyrosine (NATYR), *N*-acetyl-L-tyrosinamide (NATYRAM), L-tryptophyl-L-tyrosine (TRP–TYR dimer), horse myoglobin (Mb), and glucagon were obtained from Sigma Chemical Co. Chicken egg white lysozyme was obtained from Worthington Biochemical Co. All samples were used without further purification, and 225-nm excitation was used for the UVRR measurements. All data were obtained on a Nd:YAG pumped dye laser system operating at 20 Hz (ca. 4 nanosecond pulse width), except for several of the lowest pulse energy TRPAM, NATYR, and TRP–TYR dimer (pH 5) measurements, which derive from an excimer laser based system operated at 200 Hz. Both systems have been described in detail elsewhere.[15,16] The TRPAM, NATYR, and TRP–TYR dimer studies were carried out by using a recirculating dye laser jet nozzle sampling system which gives a sample thickness of ca. 200 μm. The Mb, lysozyme, and glucagon samples were recirculated by a peristaltic pump through 1-mm diameter quartz capillaries. The laser beam was focused with a 25-cm focal length lens. Samples were placed ca. 23 cm from the focusing optic to give beam spot sizes of ca. 1–2 mm. Pulse energies were measured with a Scientech Model 361 power meter and modulated by using Suprasil neutral density filters (Melles Griot). The Raman scattered light was collected in a backscattering geometry. A sufficient sample flow rate occurred such that the illuminated sample volume was replaced between laser pulses. The entire sample volume was replaced after each 5–10-min Raman measurement; absorption measurements before and after UV excitation revealed no spectral changes.

In order to derive ground-state repopulation rates from UVRR saturation measurements, it is necessary to determine the scaling factor which equates the total energy measured for each pulse to the effective energy flux density per pulse (millijoules/cm^2) through the sample volume which is successfully imaged into the spectrometer. We denote this effective energy flux density as I_0. I_0 is sensitive to experimental parameters such as the focusing conditions and spacial fine structure in the beam spot intensity profile as well as the sample thickness and sample absorbance. In our previous paper[14] we described the estimation of I_0 for thin samples by carefully mapping the spacial intensity distribution in the beam spot at the front face of the sample and by taking into account the attenuation of the laser beam intensity through the sample thickness. In the present studies, however, we utilize the previously demonstrated behavior of NATRPAM or TRPAM ultraviolet resonance Raman intensities as a function of I_0 as "saturation standards" to derive the effective energy flux density per pulse under each experimental condition. During each independent saturation experiment, the saturation behavior of NATRPAM or TRPAM is compared to the saturation of one of the species of interest measured under identical focusing, imaging, and sampling conditions. The absorbance at the excitation frequency for the sample of interest is made identical with that of the saturation standard solution. The concentrations used in these studies gave absorbances of ca. 1.5 per millimeter pathlength at 225 nm as in our previous report.[14] The photon counts per molecule for a nonabsorbing, nonsaturating internal intensity standard added to each sample are then compared to insure similar values of I_0. Satisfactory agreement was obtained in all cases. The absolute value of I_0 is then obtained by least-squares fitting (vide infra) of the NATRPAM or TRPAM saturation data for each experiment to give the ground-state repopulation rates previously determined for these compounds.[14]

The ultraviolet resonance Raman intensities of the absorbing analyte species were divided by the Raman intensity of the nonabsorbing internal intensity standard in each spectrum. The relative intensity ratios used here derive from peak height measurements except for the lysozyme and glucagon cases, where peak areas were utilized. No changes in vibrational bandshape were observed in any of the data reported here. The error bars indicated in the figures reflect only the error ($\pm 2\sigma$) associated with defining the relative peak height ratio within the S/N of each spectrum. In the TRPAM, NATYR, and TRP–TYR dimer saturation studies, the requirement of similar optical densities at the excitation frequency necessitated 0.4–0.5 mM sample concentrations. One molar $NaClO_4$ was used as the internal Raman intensity standard. The perchlorate cross sections at 225 nm derive from the measurements of Dudik et al.[17] The NATRPAM and horse myoglobin saturation comparison utilized 25 μM myoglobin solutions buffered with 25 mM phosphate buffer at pH 6. $NaClO_4$ (250 mM) was added as the internal intensity standard. Higher concentrations of $NaClO_4$ in the presence of phosphate buffer tended to cause some aggregation of the Mb samples. The NATRPAM solution was 200 μM in NATRPAM and 250 μM in $NaClO_4$.

Cacodylic acid was used as the internal Raman intensity standard in the lysozyme and glucagon studies. Cacodylate cross sections at 225 nm derived from relative peak area measurements in a perchlorate solution and give a cross section of 2.7 mb for the 605–628-cm^{-1} mode of cacodylate at 225 nm. The saturation behaviors of lysozyme (25 μM) and glucagon (82 μM) solutions, 60–80 mM in cacodylate, were compared to a 200 μM NATRPAM solution, 90 mM in cacodylate. The lysozyme solutions were buffered at pH 6.5. The glucagon studies were carried out at pH 10.

Results

Figure 1 shows the structures of the TRP–TYR dimer and TRPAM and NATYR monomers at pH 5. The absorption spectra of a 27 μM solution of the dimer as well as a solution containing 27 μM of each monomer are also displayed. The absorption features centered at 275 and 220 nm each consist of overlapping $\pi^* \leftarrow \pi$ absorptions from the indole and phenolic rings. The decreased molar absorptivity of the dimer throughout this spectral region derives from a hypochromic interaction[18–20]

(14) Teraoka, J.; Harmon, P. A.; Asher, S. A. *J. Am. Chem. Soc.* **1990**, *112*, 2892.
(15) Asher, S. A.; Johnson, C. R.; Murtaugh, J. *Rev. Sci. Instrum.* **1983**, *54*, 1657.
(16) Jones, C. M.; Devito, V. L.; Harmon, P. A.; Asher, S. A. *Appl. Spectrosc.* **1987**, *41*, 1268.
(17) Dudik, J. M.; Johnson, C. R.; Asher, S. A. *J. Chem. Phys.* **1985**, *82*, 1732.
(18) Tinoco, I., Jr. *J. Am. Chem. Soc.* **1960**, *82*, 4785; *J. Chem. Phys.* **1960**, *33*, 1332.
(19) Rhodes, W. *J. Am. Chem. Soc.* **1961**, *83*, 3609.

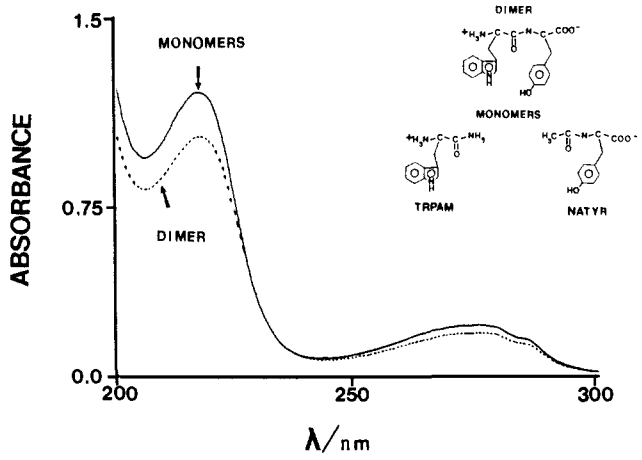

Figure 1. Absorption spectra of 27 μM TRP–TYR dimer (dashed curve) and a solution (27 μM) in both TRPAM and NATYR (solid curve) in a 1-cm pathlength cell. Structures of the monomer and dimer species are also shown.

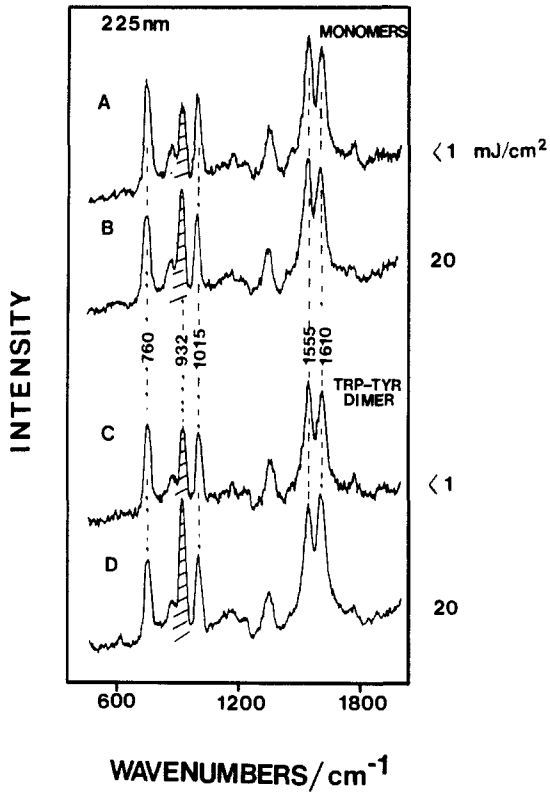

Figure 2. A 225 nm excited ultraviolet resonance Raman spectra. Spectra A and B are the NATYR/TRPAM monomer mixture at pulse energy flux density values of <1.0 and 20 mJ/cm², respectively. Spectra C and D are of the TRP–TYR dimer at pulse energy flux densities of <1.0 and 20 mJ/cm², respectively. Note changes in the analyte band Raman intensities relative to the shaded internal standard band at 932 cm⁻¹.

between the aromatic residues (vide infra).

Figure 2 displays UVRR spectra of the dimer and monomer mixture excited at 225 nm. This excitation wavelength is resonant with the allowed $B_b \leftarrow A_{1g}$ electronic transition of TRP as well as the partially allowed $L_a \leftarrow A_{1g}$ transition of the TYR ring. The spectra in Figure 2 are dominated by the Franck–Condon active totally symmetric TRP modes at 760, 1015, 1350, and 1555 cm⁻¹ in addition to the unresolved ν_{8a} and ν_{8b} TYR ring modes at ca. 1610 cm⁻¹. Spectra A and B (C and D) in Figure 2 represent different pulse energy flux density spectra of the monomer mixture (dimer). The I_o values are given on the right sides of Figure 2

(20) Bullough, R. K. *J. Chem. Phys.* **1965**, *43*, 1927.

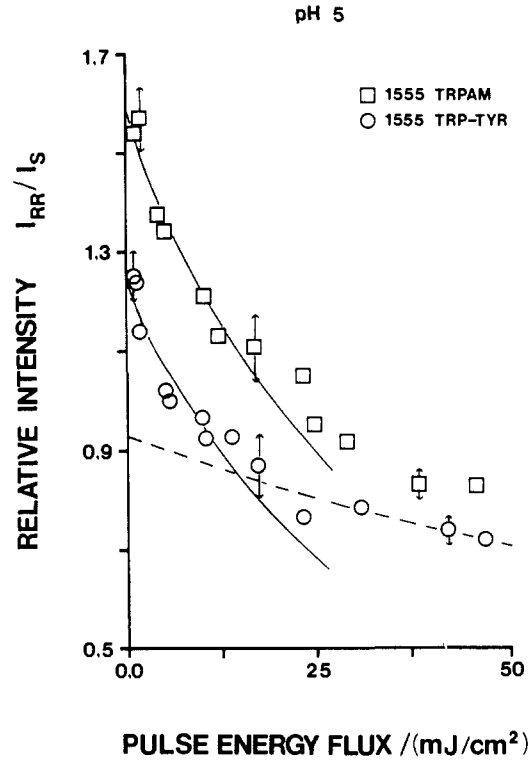

Figure 3. Plot of the 1555-cm⁻¹ tryptophan resonance Raman intensities (I_{RR}) divided by the internal standard Raman intensity (I_S) versus the effective pulse energy flux density (I_o). Open squares represent the 1555-cm⁻¹ band of TRPAM, and open circles represent the 1555-cm⁻¹ band of the TRP–TYR dimer. Relative ratios are normalized to 335 μM TRPAM or TRP–TYR and 500 mM $NaClO_4$ and are corrected for monochromator and detector responses. The relative ratio values on the ordinate axis thus correspond to Raman cross section units of b/sr-molecule.

and are derived as described above. Note the dramatically decreased relative intensities of the TRP and TYR resonance Raman intensities, compared to the nonabsorbing internal standard perchlorate band at 932 cm⁻¹, in the higher energy flux density spectra. The TRP bands have decreased ca. 40% relative to the perchlorate band, while the 1610-cm⁻¹ TYR band has decreased 20%. These decreases result from significant ground-state depletion of the absorbing TRP and TYR chromophores in the higher energy flux density spectra, due to optical absorption and the population of excited-state species which cannot rapidly relax back to the ground state on the time scale of our 4-ns laser pulse width. The nonabsorbing perchlorate ground-state concentration is independent of the pulse energy flux density. Although no new bands due to excited-state resonance Raman scattering are obvious in spectra B or D in Figure 2, a small intensity contribution underlying the 1015-cm⁻¹ ground-state TRP feature is apparent when the relative intensities of the TRP 760, 1015, 1350, and 1555 features are carefully compared in the high- and low-energy flux density spectra. The excited states or other transient species formed are evidently not as strongly enhanced at 225 nm as are the ground-state TRP or TYR.

Figure 3 plots the relative intensity ratio of the 1555-cm⁻¹ TRP band compared to the perchlorate band as a function of the pulse energy flux density I_o for both TRPAM in the monomer mixture and the TRP–TYR dimer. The TRP 760- and 1350-cm⁻¹ bands behave identically; the relative ratios of the 760-, 1350-, and 1555-cm⁻¹ bands to themselves are independent of the pulse energy flux density. In both the monomer and dimer cases, at least two different saturation behaviors (I_{RR}/I_S versus I_o) can be observed over the pulse energy flux density range plotted in Figure 3. The I_{RR}/I_S ratios initially decrease sharply but then begin to level off at higher pulse energy flux densities near ca. 20 mJ/cm². This is most easily seen by comparing the solid and dashed curves in Figure 3 which fit the eight lowest and five highest flux density 1555-cm⁻¹ TRP–TYR dimer data points, respectively. These

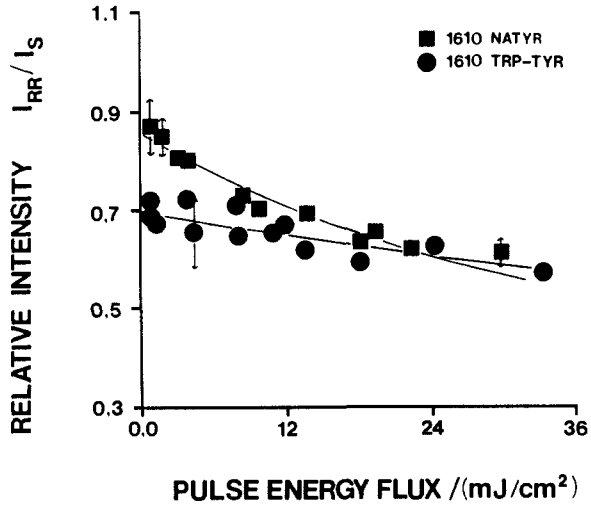

Figure 4. Plot of the 1610-cm^{-1} tyrosine resonance Raman intensities divided by the internal standard intensity versus the effective pulse energy flux density I_0: solid squares, NATYR monomer; solid circes, TRP-TYR dimer. Relative ratios normalized as described in Figure 3.

curves derive from least square fitting to a saturation model which is described below. The dashed curve clearly underestimates all lower flux density data, while the solid curve underestimates all higher flux data. The solid curves in Figures 3–5, 7, 9, and 10 can be related to intrinsic molecular relaxation rates (vide infra).

The changes in the analyte Raman intensities relative to the internal standard intensity evident in Figure 3 highlight the potential difficulties in obtaining quantitative ground-state ultraviolet resonance Raman cross sections by using pulsed laser excitation. Indeed, the highest I_0 data plotted in Figure 3 corresponds to an average power at 20 Hz of only ca. 3 mW focused to a spot size of ca. 2 mm at the sample. Quantitative cross sections can only derive from relative intensity ratios extrapolated to "zero" pulse energy flux density in such circumstances. We scaled Figures 3–5, 7, 9, and 10, such that the relative ratios are normalized to a 335 μM concentration of TRP or TYR residue and 500 mM $NaClO_4$ and have been corrected for monochromator and detector wavelength dependencies and the perchlorate Raman cross section. Thus, the values of the intensity ratios in these figures can be directly read off as 225-nm excitation Raman cross sections in units of b/sr-molecule.

The saturation behaviors of the 1610-cm^{-1} TYR vibrations in the monomer mixture and the TRP–TYR dimer are shown in Figure 4. We deconvolute the 1610- and 1555-cm^{-1} bands by independent measurements of TRPAM and NATYR resonance Raman spectra and assume the same overlap in the dimer vibrational spectra. This gives a 13% contribution of TYR vibrational intensity at 1555 cm^{-1} (relative to that at 1610 cm^{-1}) and a 35% contribution of TRP vibrational intensity at 1610 cm^{-1} (relative to that at 1555 cm^{-1}). Solving simultaneous equations gives the 1610- and 1555-cm^{-1} peak heights. Figure 4 shows that the saturation is clearly different for the NATYR monomer than for the TYR residue in the TRP–TYR dimer. The ratio of the dimer 1610-cm^{-1} Raman intensity to the perchlorate internal standard intensity decreases more slowly with increasing I_0 than occurs in the monomer case indicating a smaller extent of ground-state depletion. Only a single monotonic decrease in the relative intensities is obvious in contrast to the behavior evident in Figure 3.

Shown in Figure 5 are the saturation of the 1555- and 760-cm^{-1} TRP bands of the dimer and TRPAM in the monomer mixture at pH 12, where the TYR phenolic group is deprotonated as is the TRPAM N-terminal amino group. The TYR $\pi^* \leftarrow \pi$ transitions are in this case red-shifted from 220 and 275 nm to ca. 240 and 295 nm, respectively. The smaller slopes of the dimer intensity ratios in Figure 5 indicate that at this basic pH, a reduced ground-state depletion occurs for the TRP chromophore in the dimer compared to that in the TRPAM monomer. Clearly different Raman cross sections are observed between the monomers and the TRP–TYR dimer in Figures 3–5. Note that the pulse energy flux density range is lower than that of Figures 3 and 4.

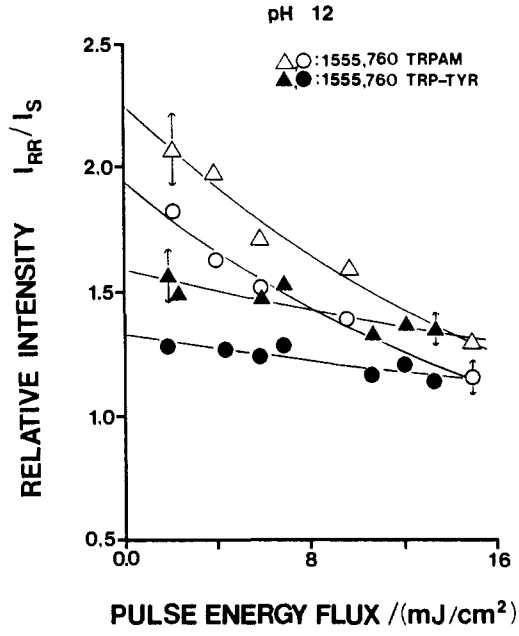

Figure 5. Plots of the 1555- and 760-cm^{-1} tryptophan intensities relative to the internal standard intensity for the monomer mixture (open triangles and open circles, respectively) and for the TRP–TYR dimer (solid triangles and solid circles) at pH 12 versus I_0. Relative ratios normalized as in Figures 3 and 4.

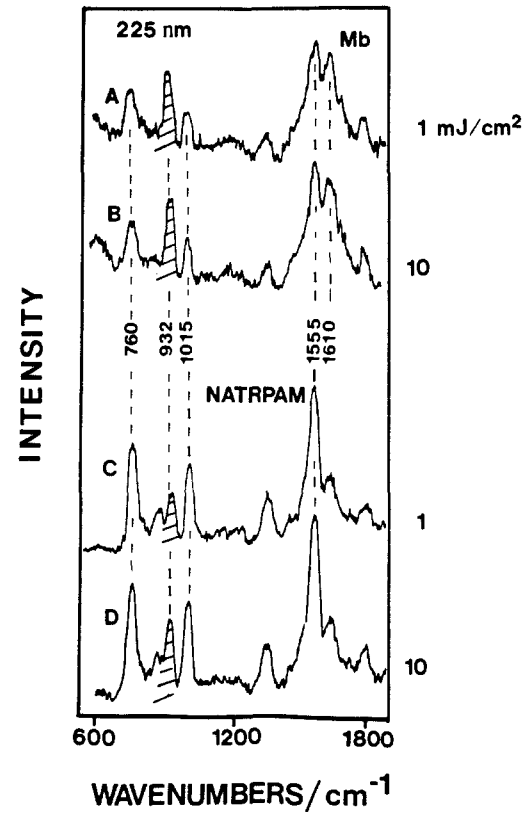

Figure 6. A 225 nm excited ultraviolet resonance Raman spectra of myoglobin (spectra A and B) and NATRPAM (spectra C and D) at different I_0 values. I_0 values are indicated on the right side. Compare the analyte band Raman intensities relative to the shaded internal standard band intensities in the lower and higher pulse energy flux density spectra.

Figure 6 shows different pulse energy flux density spectra of Mb (spectra A and B) and NATRPAM (spectra C and D) obtained under identical experimental conditions. At 225 nm, the

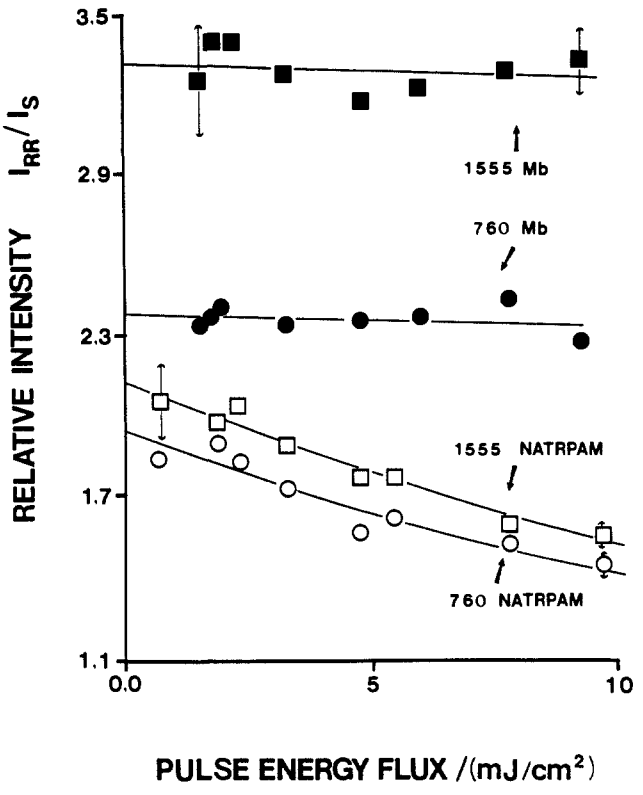

Figure 7. Plots of the 1555- and 760-cm^{-1} tryptophan intensities in Mb (solid squares and solid circles) and for NATRPAM (open squares and open circles) relative to the internal standard. Note I_0 pulse energy flux density range plotted is significantly lower than for Figures 3 and 4. Relative ratios normalized to 335 μM tryptophan residue in Mb and 335 μM NATRPAM against 500 mM $NaClO_4$ as described previously.

two TRP and two TYR residues in horse Mb are selectively enhanced and completely dominate the protein UVRR spectrum, which resembles the monomer mixture or the TRP–TYR dimer spectra in Figure 2. Little if any decrease in the Mb TRP or TYR residue band intensities relative to the internal standard band is observed in the higher I_0 excited spectrum B, compared to the lower excited I_0 spectrum A. In contrast, the NATRPAM spectra C and D in Figure 6 show significant changes. Figure 7 displays plots similar to Figures 3–5 for the 1555- and 760-cm^{-1} bands of NATRPAM and the two TRP residues in Mb. The weak dependence of the Mb 1555- and 760-cm^{-1} relative intensity ratios on I_0 indicated in Figure 7 clearly shows that little ground-state depletion occurs for the TRP residues in the Mb protein compared to NATRPAM. These differences in saturation behavior as well in Raman cross sections must be related to the protein environment surrounding the TRP side chains and is discussed further below.

Figure 8 displays different pulse energy flux density 225 nm excited Raman spectra of the 28 residue polypeptide glucagon (spectra A and B) as well as lysozyme (spectra C and D). Glucagon has one TRP and two TYR residues, while lysozyme has six TRP and three TYR residues. The substantial changes in the intensities of the TRP bands relative to the internal intensity standard cacodylate band at 605 cm^{-1} in spectra A and B demonstrate ground-state depletion of the TRP residues during the laser pulse in glucagon. Differences between ground-state depletion of the TRP and TYR residues is also evident. This is most easily seen by the complete reversal of the 1555-cm^{-1} TRP side-chain mode and the 1610-cm^{-1} TYR side-chain band relative intensities between spectra A and B. The less dramatic relative intensity changes in spectra C and D indicate that averaged over the six TRP residues in lysozyme, the TRP residues in lysozyme show less ground-state depletion than the single TRP residue in glucagon. Figure 9 shows plots of I_{RR}/I_S versus I_0, for the 1555- and 760-cm^{-1} TRP bands of glucagon and lysozyme. The larger slopes for the glucagon TRP mode relative ratio plots indicate a more extensive ground-state depletion than occurs for lysozyme.

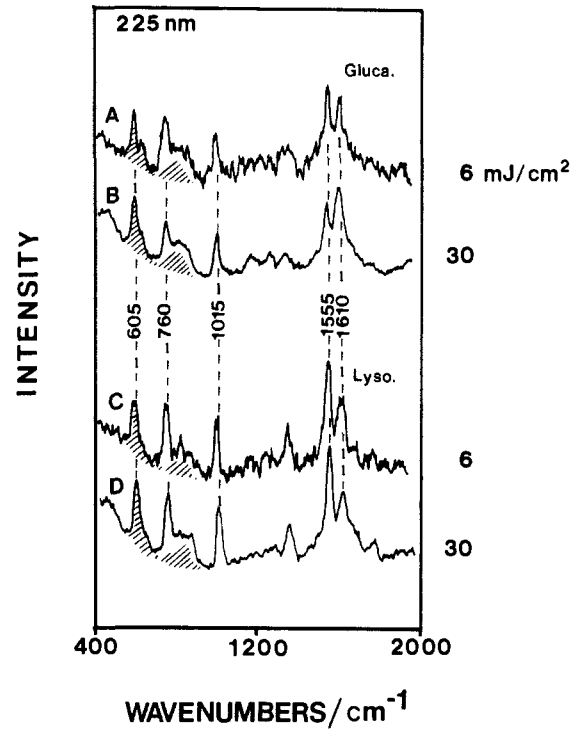

Figure 8. A 225 nm excited ultraviolet resonance Raman spectra of glucagon (spectra A and B) and lysozyme (spectra C and D) at different pulse energy flux densities. I_0 values are given on the right. Note the changes in intensities of the protein bands compared to the shaded cacodylate internal standard band at 605 cm^{-1}.

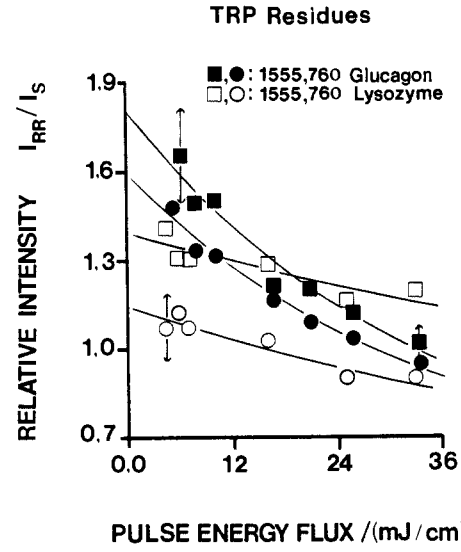

Figure 9. Plots of the tryptophan 1555- and 760-cm^{-1} bands relative intensity ratios for glucagon (solid squares and solid circles) and lysozyme (open squares and open circles) versus I_0. Ratios normalized to 335 μM glucagon, 335 μM tryptophan residue in lysozyme, and 125 mM cacodylate to permit the ordinate axis to be read off in average Raman cross sections in b/sr-molecule.

However, the TRP side chains of lysozyme exhibit more ground-state depletion than those in myoglobin. Differences in TRP side chain mode Raman cross sections in glucagon and lysozyme are obvious from the fits giving the I_{RR}/I_S values at zero pulse energy flux density. Examination of Figure 9 reveals, however, that these intrinsic cross section differences between proteins can become completely masked by differences between their ground-state depopulation at high pulse energy flux densities.

Figure 10 shows similar plots for the TYR 1610-cm^{-1} features in Mb, glucagon, and lysozyme. Myoglobin and glucagon TYR residues show little ground-state depletion, while the three TYR residues in lysozyme show significant ground-state depletion over

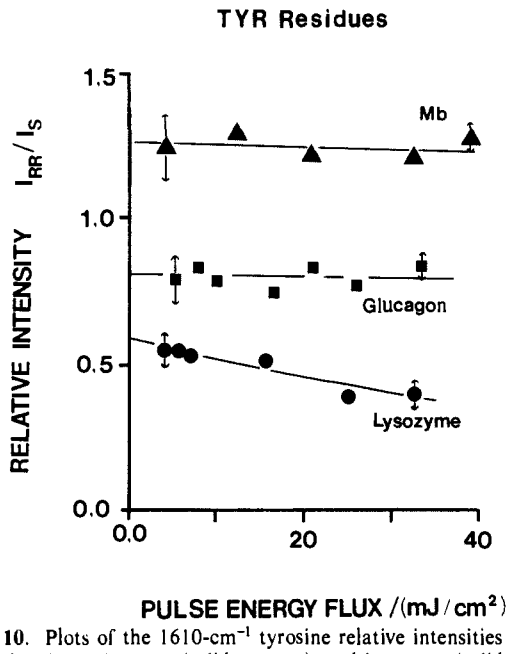

Figure 10. Plots of the 1610-cm^{-1} tyrosine relative intensities for Mb (solid triangles), glucagon (solid squares), and lysozyme (solid circles) versus I_o.

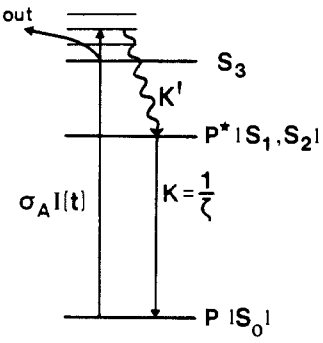

Figure 11. Scheme for ground-state depopulation and excited-state population and relaxation for 225-nm excitation of tryptophan and tyrosine chromophores in condensed phases. See text for details.

the I_o range plotted in Figure 10. The TYR cross sections in Figure 10 for glucagon derive from the approximation that 40% of the TYR residues are ionized to tyrosinate at pH 10 and do not contribute significantly to the 1610-cm^{-1} feature with 225-nm excitation.[21]

Discussion

Photophysical Model for Saturation. In a previous paper[14] we introduced a simple model which quantitatively described the decrease in the I_{RR}/I_S relative ratios versus pulse energy flux observed for a series of simple TRP derivatives excited at 225 nm in aqueous solutions. In this model, the ground state is depleted via optical absorption which populates excited electronic states. The ground-state repopulation rate is determined by the rate of excited electronic state relaxation back to the ground state during the laser pulse. The Raman saturation methodology is most sensitive to relaxation "lifetimes" which are on the order of the laser pulse width, which in the present case is ca. 4 ns. The saturation model is shown in Figure 11. σ_A is the absorption cross section at the excitation frequency (cm^2/photon), $I(t) = I_p L(t)$ describes the laser pulse intensity at time t. I_p (photons/cm^2) is the pulse photon flux density, which is simply the quantity I_o as defined in the Experimental Section divided by the photon energy in mJ. $L(t)$ is a normalized temporal laser pulse shape function. We have found that $L(t)$ can be taken to be a rectangular "on–off" function without introducing significant error.[14] The product $\sigma_A I(t)$ therefore defines the rate at which the ground state is depopulated during the laser pulse. In the general case, S_3 represents the resonant excited electronic states. K' is the rate constant for rapid internal conversion in the condensed phase to the lowest lying electronic state(s) (S_1 and S_2 in Figure 11) from which fluorescence and nonradiative relaxations repopulate the ground state with a total rate given by K. ϕ_{oul} allows for some fraction of molecules to populate states long lived compared to our laser pulse width, prior to internal conversion to fluorescing levels. We consider the typical case in the condensed phase where $K' \gg K$. It can be shown that in this limit the excitation–relaxation scheme in Figure 11 predicts a pulse energy (or photon) flux density dependence of the I_{RR}/I_o ratio for each vibrational mode of the absorbing analyte given by[14]

$$\frac{I_{RR}}{I_S} = \frac{\sigma_R p_o}{\sigma_S C_o}\left[\frac{1}{\phi_{oul}\sigma_A I_p} + \frac{(2\phi_{oul}\sigma_A I_p - Kt_o - \sigma_A I_p - F^{1/2})e^{1/2(-(Kt_o+\sigma_A I_p)+F^{1/2})}}{2\phi_{oul}\sigma_A I_p F^{1/2}} - \frac{(2\phi_{oul}\sigma_A I_p - Kt_o - \sigma_A I_p + F^{1/2})e^{1/2(-(Kt_o+\sigma_A I_p)-F^{1/2})}}{2\phi_{oul}\sigma_A I_p F^{1/2}}\right] \quad (1)$$

where $F = (Kt_o + \sigma_A I_p)^2 - 4\phi_{oul} Kt_o \sigma_A I_p$ and σ_R and σ_S (P_o and C_o) are the analyte and internal standard Raman cross sections (concentrations), respectively. If $\phi_{oul} = 0$ in Figure 11, the internal conversion efficiency is 100%. Equation 1 becomes undefined for $\phi_{oul} = 0$; we showed previously that in this case eq 1 becomes

$$\frac{I_{RR}}{I_S} = \frac{\sigma_R P_o}{\sigma_S C_o(\sigma_A I_o + Kt_o)^2}\{(Kt_o)^2 + \sigma_A I_o(1 + Kt_o - \exp[-(\sigma_A I_o + Kt_o)])\} \quad (2)$$

σ_A is either directly measured from the absorption spectrum or estimated in more complex cases from the resonance Raman cross sections (vide infra). I_o (or equivalently I_p) is derived from the saturation response of the NATRPAM or TRPAM "saturation standards" as discussed in the Experimental Section. In eqs 1 and 2, we can least-squares fit two variables from the I_{RR}/I_S versus I_o Raman data. In eq 1, we least-squares fit the variable σ_R, which is proportional to I_{RR}/I_S at zero pulse energy flux density, and either ϕ_{oul} or K. K can be uniquely fit if ϕ_{oul} is defined and vice versa. In eq 2, σ_R and K are least-squares fit.

It should be emphasized that with the present UV Raman signal-to-noise ratios, eqs 1 and 2 give statistically identical fits to our I_{RR}/I_S versus I_o data. Equation 1, for example, with ϕ_{oul} = 100% and an infinitely large value for K will predict identical I_{RR}/I_S versus I_o behavior as eq 2 with an infinitely small value for K. The choice as to whether or not to allow ϕ_{oul} to take on nonzero values is determined by initially comparing our derived value of K by using eq 2, which assumes $\phi_{oul} = 0$, with the available fluorescence lifetime data. For example, we found the 225-nm saturation behaviors for NATRPAM and TRPAM (pH > 9) are modeled by eq 2 ($\phi_{oul} = 0$) and ground-state repopulation rates of $K = 1/(2.9 \pm 0.5)$ and $1/(7.1 \pm 1.4)$ ns^{-1}, respectively.[14] These results are consistent with the known fluorescence lifetimes of S_1/S_2 of 3 and 7 ns.[22] The agreement between the 225-nm excited Raman saturation values and the lowest excited-state fluorescence lifetimes indicate an efficient (essentially 100%) internal conversion to fluorescing levels from 225 nm. This result precludes the use of eq 1 and also indicates that the fluorescence decay rates are dominated by direct repopulation of ground-state species which are rapidly thermalized (compared to our laser pulse width). Thus, intersystem crossing and photoionization contributes negligibly to the fluorescing excited-state decay rates. This is consistent with TRP derivative measurements of triplet and photoionization quantum yields from fluorescing levels, which together are less than ca. 10%.[23]

(21) Gratzer, W. B.; Beaven, G. H. *J. Biol. Chem.* **1969**, *244*, 6675.

(22) Petrich, J. W.; Chang, M. C.; McDonald, D. B.; Fleming, G. R. *J. Am. Chem. Soc.* **1983**, *105*, 3824.

In the case of TRPAM (pH 5), however, eq 2 gave K values much slower than the fluorescence decay rates. Thus, we utilized eq 1 and found that a nonzero value of $\phi_{oul} = 0.55$ was required for the fitted value of K to agree with the time-resolved fluorescence lifetime of ca. 1.5 ns. We associate these ϕ_{oul} values with the significant decreases in fluorescence quantum yields, concomitant with large increases in solvated electron formation, which have been demonstrated for a few TRP and TYR derivatives at excitation wavelengths shorter than 240 nm.[23] ϕ_{oul} in such a case would reflect formation of TRP or TYR radical species with lifetimes of the order of microseconds. For the studies here we use eq 1 and these previous results to determine the effective I_o under the present experimental conditions.

Estimation of σ_A Values for TRP and TYR Residues. The excitation/relaxation scheme shown in Figure 1 and described by eq 1 or 2 requires the value of the absorption cross section, σ_A at the laser excitation frequency. Over- or underestimation of σ_A will lead to proportional over- or underestimation of ground-state repopulation rates. In our previous study of TRP derivatives as well as in the case NATYPAM, TRPAM (pH 5, pH 9), and NATYR reported here, σ_A at 225 nm is simply measured from the absorption spectrum. In the TRP–TYR dimer and in glucagon, myoglobin, and lysozyme, however, the absorbance at 225 nm has significant contributions from TRP and TYR residues as well as other protein components. Simple measurement of TRP and TYR σ_A values is therefore not possible from the absorption spectrum. We estimate the protein σ_A values by noting that the electron-nuclear coupling for the indole chromophore in NATRPAM, for example, is expected to be similar to that for a TRP residue in a protein. The Franck–Condon or "A-term" enhanced resonance Raman intensity of NATRPAM compared to a TRP residue in a protein might therefore be expected to scale quadratically within the absorption cross section at the laser excitation frequency. We found previously, for example, that the difference in 225-nm resonance Raman cross sections for a number of TRP derivatives was quantitatively proportional to the square of the respective 225-nm molar absorbtivities. In this manner, the fitted zero pulse energy flux density I_{RR}/I_S ratios are compared for NATRPAM and the TRP residues in myoglobin, lysozyme, and glucagon to estimate the TRP σ_A protein values. In an exactly analogous manner, we utilize the 225-nm excited NATYRAM resonance Raman cross sections to estimate the protein TYR residue σ_A values. In the case of the TRP–TYR dimer, the TRP and TYR residue Raman cross sections were compared to TRPAM and NATYR, respectively, to estimate σ_A values for each chromophore in the dimer. It should be noted that at pH 5 the Raman cross sections indicate an ca. 10% hypochromic decrease in both the TRP and TYR σ_A values in the dimer near 225 nm which is consistent with the absorption spectra displayed in Figure 1.

A final comment regarding the estimation of σ_A values from Raman cross sections is warranted. It would seem that the least-squares fit for the zero pulse energy flux density I_{RR}/I_S value, which is proportional to the Raman cross-section σ_R, should be sensitive to the estimate value for σ_A. Fortunately this is not so. For a given I_{RR}/I_S versus I_o data set, we obtain essentially identical fits for I_{RR}/I_S at zero pulse energy flux density for a wide range of initial input σ_A guesses, the differences being in the resulting fitted values of K. We therefore start with a reasonable guess of σ_A, obtain the fitted I_{RR}/I_S ratio at zero pulse energy flux density, recalculate the σ_R, and derive the correct σ_A value. This iterated σ_A value is used to extract the reported values for K.

Monomer–Dimer Saturation Behavior. The monomer mixture and TRP–TYR dimer represent a simple model system to determine if the Raman saturation methodology can probe changes in ground electronic state repopulation rates which derive from interresidue interactions. Clearly the saturation methodology must be sensitive to these types of interactions if it is to be useful in examining chromophore environments in proteins. Differences in the ground-state recovery rates between the monomers and the TRP–TYR dimer should derive from interactions between the aromatic side chains which are in close proximity to each other in the dimer. Singlet–singlet energy transfer has been observed in TRP–TYR dimer to give quenching of the steady-state TYR fluorescence intensity at neutral pH.[24] The TYR fluorescence intensity increases in peptides as the average distance between the TRP and TYR residues increases by the insertion of glycine residues between the TYR and TRP.

The theory for this energy transfer has been well-developed by Förster and others.[25-27] Energy transfer in condensed phase systems occurs primarily between the lowest singlet excited states. Energy transfer can occur if the absorption of one chromophore (the acceptor) overlaps the emission spectrum of the other (the donor). Before energy transfer, the donor is in the fluorescent excited state, while the acceptor is in the ground state. After energy transfer, the donor has relaxed to the ground state while exciting the acceptor to a nearly isoenergetic electronic excited state. The energy is transferred via a dipole–dipole interaction and has a $1/(r)^6$ as well as an orientational dependence. At neutral and acidic pH, the energies of the TYR and TRP absorption and emission transitions require that the direction of energy transfer be from TYR to TRP. The energy-transfer rate for TYR and TRP chromophores 15-Å apart has been calculated to be equal to the combined rates for all other processes removing molecules from the TYR fluorescing levels.[28]

A second type of interaction which alters excited-state relaxation rates and therefore ground-state recovery rates in the TRP–TYR dimer from that in the monomers involves differences in the nearness of approach of C or N terminal quenching groups or peptide bonds to the TYR and TRP aromatic rings. For example, although the total decay rate from fluorescing levels of the monomer TRPAM (pH 5) and TRP–glycine dimer are similar,[22] the fluorescence decay of NATYR is $1/3.5$ ns^{-1} while for glycine–TYR dimer the fluorescence decay rate is $1/1.6$ ns^{-1}.[29]

The data in Figure 4 indicate that changes in ground-state repopulation rates exist between the monomer and dimer. Since the absorption cross sections of the NATYR monomer and the TYR residue in the dimer are similar, the less rapid decrease in the I_{RR}/I_S relative ratios versus pulse energy flux density in the dimer indicates a more rapid ground-state recovery rate. The solid curve in Figure 4 for the NATYR data derives from a least-squares fitting of the I_{RR}/I_S ratios with eq 2 ($\phi_{oul} = 0$) and the measured absorption cross section $\sigma_A = 3.4 \times 10^{-17}$ cm^2/photon. The fitted value for the ground-state recovery rate K gives $1/5.5$ ns^{-1}, which is somewhat slower than the fluorescing excited-state decay rate of $1/3.5$ ns^{-1}.[29] The discrepancy probably derives from significant triplet yields from fluorescing levels and/or monophotonic photoionization from excited states near 225 nm prior to internal conversion to fluorescing states. The use of ϕ_{oul} values around 20‰ in eq 1 results in K values near $1/3.5$ ns^{-1}.

The least-squares-fitted solid curve in Figure 4 for the dimer TYR residue 1610-cm^{-1} band, however, gives a much faster ground-state recovery rate of $1/0.7$ ns^{-1}. The dimer curve shown in Figure 4 derives from eq 2 with $\sigma_A = 3.0 \times 10^{-17}$ cm^2/photon. This value of σ_A is 10% smaller than the NATYR monomer value as discussed above. This ca. 7-fold increase in the tyrosyl residue ground-state repopulation rate is expected due to the occurrence of TYR to TRP singlet energy transfer in the dimer.

The TRPAM monomer and TRP dimer residue saturation data in Figure 3 have purposely been measured over a pulse energy flux range where photon driven relaxations begin to contribute

(23) Creed, D. *Photochem. Photobiol.* **1984**, *39*, 537, 563.

(24) Edelhoch, H.; Perlman, R. L.; Wilchek, M. *Biochemistry* **1968**, *7*, 3893.

(25) Forster, T. In *Modern Quantum Chemistry*; Sinanoglu, O., Ed.; Academic: New York, 1965; Vol. 3, pp 93-137.

(26) Stryer, L.; Haugland, R. P. *Proc. Natl. Acad. Sci. U.S.A.* **1967**, *98*, 719.

(27) Fairclough, R.; Cantor, C. R. In *Methods of Enzymology*; Hirs, C. H., Timasheff, S. N., Eds.; Academic Press: New York, 1977; p 347.

(28) Perlman, R.; Van Zyl, A.; Edelhoch, H. *J. Am. Chem. Soc.* **1968**, *90*, 2168.

(29) Laws, W. R.; Ross, J. B. A.; Wyssbrod, H. R.; Beechem, J. M.; Brand, L.; Sutherland, J. C. *Biochemistry* **1986**, *25*, 599.

significantly to the ground-state repopulation rates. The "turning on" of these processes is seen in Figure 3 near ca. $I_o = 20$ mJ/cm^2 by the decreased dependence of the I_{RR}/I_S ratios on I_o. We showed previously that this process derives from amplified spontaneous emission (ASE) from the lowest energy singlet fluorescing levels. Since ASE requires a population inversion, ASE can increase ground-state recovery rates only when the ground-state population becomes more than 50% depleted by the end of the laser pulse. By using the laser pulse shape function and the population rate equations leading to eqs 1 and 2, we calculate that when the apparent ground-state population (determined from the Raman intensity averaged over the laser pulse duration) is reduced by 30%, ASE begins to occur by the end of the laser pulse. Indeed, the I_{RR}/I_S versus I_o plots consistently manifest the change in initial slope for I_{RR}/I_S values reduced by ca. 30% from their maximum values.

Thus, we can confidently extract intrinsic ground-state repopulation rates from I_{RR}/I_S versus I_o data by using those I_{RR}/I_S data which are reduced by less than 30% from the maximum relative intensity ratio value. Obviously, chromophores with the largest absorption cross sections and the longest excited-state lifetimes will exhibit this ASE interference at the lowest pulse energy fluxes. This is why all the TYR data of Figure 4 are modeled well by eq 2 and can be used in fitting ground-state recovery rates, while for the TRP chromophores in Figure 3, which have absorption cross sections more than two times larger, we can only utilize the eight lower pulse energy flux data. These fits are shown by the solid curves in Figure 3 which grossly underestimate the higher pulse energy flux density I_{RR}/I_S ratios.

TYR to TRP energy transfer should result in an increased TRP saturation in the dimer in the lowest energy flux density regimes. This is consistent with the dimer data of Figure 3. The solid curve through the TRPAM data derives from eq 1 with $\phi_{oul} = 0.55$ and $K = 1/1.5$ ns^{-1} as described previously. To facilitate comparison to TRPAM, we assume that in the dimer TRP residue case, $\phi_{oul} = 0.55$. The solid curve fit to the dimer TRP data thus derives from eq 1 with a fitted value of $K = 1/2.5$ ns^{-1}. The slower ground-state repopulation rate for the TRP in the dimer would suggest TYR to TRP energy transfer. The differences between the monomer and dimer TRP saturation is expected to be modest since energy transfer from TYR to TRP in the dimer will not dominate the TRP residue ground-state recovery in the dimer. The 2-fold larger TRP compared to TYR absorption cross section causes a 2-fold higher rate of TRP transfer into the excited state even in the absence of energy transfer.

The effect of energy transfer on TRP saturation behavior is readily apparent at basic pH conditions (Figure 5) where the TYR side chain is deprotonated. The deportonation results in a significant red-shift of the TYR 220 and 270 nm L_a and L_b $\pi \rightarrow \pi^*$ transitions to 240 and 300 nm, respectively. An examination of the TRP and tyrosinate absorption spectra indicates that the direction of energy transfer should be reversed, proceeding from TRP to TYR in the dimer. Cowgill[30] has shown in steady-state fluorescence studies of peptides containing both TRP and TYR that ionization of the TYR causes quenching of TRP fluorescence, presumably due to TRP to tyrosinate energy transfer. The TRP to tyrosinate energy transfer is evident in Figure 5 since the dimer TRP bands at pH 12 show less saturation and faster ground-state repopulation rates than present for the TRPAM monomer. Differences in C or N terminal group or peptide bond quenching interactions between the TRPAM monomer and the dimer are negligible at basic pH since TRPAM and TRP–glycine have similar fluorescence decays at pH > 9. The solid curve for the 1555- and 760-cm^{-1} TRPAM modes in Figures 5 define the I_o axis and derive from eq 2 ($\phi_{oul} = 0$) with $\sigma_A = 8.6 \times 10^{-17}$ cm^2/photon and $K = 1/7.8$ and $K = 1/6.0$ ns^{-1}, respectively. These K values are identical within the statistics of the fit. The fitted curves to eq 2 for the dimer 1555- and 760-cm^{-1} TRP bands at basic pH shown in Figure 5 give $K = 1/0.8$ and $K = 1/0.6$ ns^{-1} with $\sigma_A = 7.0 \times 10^{-17}$ cm^2/photon (derived from the Raman cross sections). This faster ground-state recovery rate of ca. 1/0.7 ns^{-1} indicates an ca. 10-fold increase in the TRP ground-state repopulation rate in the TRP–TYR dimer compared to TRPAM at basic pH.

Figures 3–5 indicate a decrease in the Raman cross sections of the dimer compared to the monomers. The relative cross-section ratios at zero pulse energy flux in Figure 3 and 4 show dimer/monomer Raman cross-section ratios of 0.77 and 0.82, respectively. The data in Figure 5 at basic pH give a similar dimer/monomer cross-section ratio of 0.70. These Raman cross-section decreases reflect the reduced molar absorbtivity of the dimer in the 225-nm spectral region as observed in the Figure 1 absorption spectra. The reduced absorption intensity originates from hypochromic interactions[18-20] between the aromatic side chains in the dimer which involves an interaction between the induced dipoles of adjacent chromophores which depresses the lower energy transition moments. In the case where the resonance Raman intensity derives primarily from the resonant electronic transition (Franck–Condon allowed or "A-term" enhancement), the resonance Raman intensity will scale quadratically with the oscillator strength. Thus, the dimer/monomer cross-section ratios can be used to estimate the hypochromic absorption changes for each chromophore of the dimer. Thus, at pH 5, both the TRP and TYR chromophores undergo an ca. 10% hypochromic absorption decrease near 225 nm. At basic pH, the dimer/monomer cross-section ratio of 0.70 gives an ca. 17% hypochromic absorption decrease for the TRP in the dimer (hence the value of $\sigma_A = 0.078$ used for the generation of the solid curves in Figure 5).

Myoglobin TRP and TYR Residue Saturation. The utility of the Raman saturation methodology in probing aromatic amino acid residue ground state repopulation rates in proteins was tested by examining the saturation behavior of the TRP and TYR residues in the heme protein myoglobin. The TRP fluorescence from heme proteins is strongly quenched due to energy transfer to the heme.[31] The energy transfer occurs over fairly large distances due to the large overlap of the TRP emission and heme absorption spectra. In the horse Mb examined here, for example, TRP 7 and TRP 14 are ca. 20 and 15 Å from the heme macrocycle.[32] The fluorescence decay components of these two TRP residues in sperm whale Mb, which has an X-ray structure similar to horse Mb, have been time resolved. The two major decay components suggest 53% of the TRP residues relax with a 1/16-ps^{-1} rate and 39% with a 1/135-ps^{-1} rate.[33] The utility of the Raman saturation methodology to monitor these ground-state recovery rates is evident in Figure 7 where the weak dependence of the I_{RR}/I_S ratios on I_o for the TRP residues in horse Mb clearly reflect the rapid ground-state repopulation via energy transfer to the heme. The fits to eq 2 of the 760- and 1555-cm^{-1} indole mode saturation data in Mb with $\sigma_A = 11.0 \times 10^{-17}$ cm^2/photon (a 25% increase from the NATRPAM σ_A value, based on the Raman cross-section differences in Figure 7) give ground-state repopulation rates of $K = 1/70$ ps^{-1}. This single ground-state recovery rate modeled by eq 1 is consistent with similar populations of emitters with ca. 1/20- and 140-ps^{-1} relaxation rates as indicated by the fluorescence measurements.[33] It should be pointed out that although the Mb TRP I_{RR}/I_S ratios do not change dramatically over the low flux density range plotted in Figure 7, significant TRP ground-state depletion would occur under higher flux conditions. The fit to the Mb TRP data in Figure 7 predicts that at $I_o = 120$ mJ/cm^2, for example, the measured I_{RR}/I_S value will be 20% less than that at zero pulse energy flux density. A pulse energy flux density value of 120 mJ/cm^2 is achieved with 1 mW of average power (20 Hz) focused to an ca. 150 micron spot size at the sample.

The TYR 103 and TYR 146 residue ground-state recovery rates in horse Mb are also quite rapid as seen from the data in Figure 10. Note that the TYR data in Figure 10 extends over a larger I_o range than the TRP Mb data in Figure 7. The solid curve which

(30) Cowgill, R. W. *Biochem. Biophys. Acta* **1963**, *75*, 272.

(31) Weber, G.; Teale, F. J. W. *Discuss. Faraday Soc.* **1959**, *27*, 134.
(32) Edmundson, A. B. *Nature* **1965**, *205*, 883.
(33) Hochstrasser, R. M.; Negus, D. K. *Proc. Natl. Acad. Sci. U.S.A.* **1984**, *81*, 4399.

fits the TYR residue I_{RR}/I_0 relative ratios gives a ground-state recovery rate of 1/40 ps^{-1} in eq 2 with $\sigma_A = 4.0 \times 10^{-17}$ cm^2/photon (derived from the Raman cross sections). This represents to our knowledge the first measurement of TYR residue excited-state relaxation rates in a heme protein. It is questionable if the fitted TYR ground-state recovery rate is significantly different from the 1/70 ps^{-1} myoglobin TRP recovery rate within the statistics of our data, particularly considering the fact that our laser pulse width is considerably longer than these relaxation times. The energy-transfer rate for the TYR residues is however likely to be faster than the TRP residues since both the TYR are within ca. 10 Å of the heme, whereas the TRP are ca. 15–20 Å from the heme.

Lysozyme and Glucagon Saturation. Lysozyme is a small non-heme, globular protein (molecular weight ca. 14 KD) containing six TRP and three TYR residues. Since lysozyme has no heme, we expect TRP and TYR ground-state recovery rates slower than that in Mb. Fluorescence studies of lysozyme at neutral pH have shown, however, that most of the TRP residues are partially quenched. The fluorescence data indicate that five of the six TRP side chains in lysozyme have lifetimes of ca. 0.4–0.5 ns, while the remaining residue exhibits an ca. 2.3-ns lifetime that dominates the total observed fluorescence intensity.[34] The fluorescence quenching derives at least in part from TRP–TRP energy transfer and from the large contact areas of three of the TRP residues with nearby disulfide bonds which can quench TRP fluorescence over short distances.[35,36] The best fit solid curves in Figure 9 through the lysozyme 760- and 1555-cm^{-1} TRP bands which derive from eq 2 with $\sigma_A = 7.2 \times 10^{-17}$ cm^2/photon (ca. 20% less than the NATRPAM σ_A value based on the Raman cross-section differences) give $K = 1/(0.4 \pm 0.1)$ ns^{-1}. The lysozyme TRP residue saturation results are consistent with the fluorescence decay data, when it is realized the I_{RR}/I_S ratios have essentially identical contributions from each TRP residue regardless of its relaxation rate. Our observed ground-state recovery rates are dominated by the five more rapidly relaxing TRP residues.

The lysozyme TYR residue saturation data in Figure 10 suggest ground-state recovery rates considerably slower than that of the TRP residues. The fitted solid curve in Figure 10 for the TYR residues in lysozyme give a ground-state recovery rate of $K = 1/6.0$ ns^{-1} by using eq 2, which is similar to that measured for NATYR in Figure 4. This result indicates no major quenching processes for the TYR residues. No time-resolved measurements or reliable quantum yields[37] for TYR emission from lysozyme are available for comparison. Saito et al.[38] have estimated the TYR-to-TRP energy-transfer rates in a number of proteins, by simultaneously monitoring fluorescence and absorbance. Their results for the TYR residues in lysozyme show a TYR-to-TRP energy-transfer efficiency of ca. 50 ± 30%. Our TYR ground-state recovery rates are consistent with the lower limits of Saito et al.'s TYR-to-TRP energy-transfer estimates.

Glucagon is a 29 residue peptide hormone containing one TRP at position 25 and two TYR at positions 10 and 13. In dilute concentrations similar to those employed here, glucagon adopts a predominantly extended flexible random coil conformation except for a nonrandom structure for residues 22 to 25.[39] Under the pH 10 conditions employed here, the spectrophotometric titration curves of Gratzer et al.[21] indicate that ca. 40% of the TYR residues in glucagon are ionized. These tyrosinates could provide TRP energy acceptor sites but are too distant from TRP 25 for efficient transfer. Thus, little TRP energy transfer is expected. This is born out by the sharply decreasing I_{RR}/I_S relative ratios in Figure 9. The solid curve fits of eq 2 to the glucagon data give the TRP ground-state repopulation rate of $K = 1/(1.6 \pm 0.3)$ ns^{-1}. The reported double exponential fluorescence decay parameters for TRP emission in glucagon show a considerable variation, ranging from 65% of a 0.5-ns component and 35% of a 3.3-ns component to 53% of a 1.5-ns component and 47% of a 4.1-ns component.[40,41] The most reliable values, measured at concentrations and pH conditions similar to our study, give approximately equal contributions of ca. 3.3- and 1.1-ns decay components.[42,43] Since exponential decays do not simply average, the double exponential fluorescence decay can be compared to our single repopulation rate if we assume that the different emitters have identical Raman cross sections. We then simply add population weighted I_{RR}/I_S versus I_0 "responses" calculated via eq 1 for 1/3.3- and 1/1.1-ns^{-1} repopulation rates. The resulting total I_{RR}/I_S versus I_0 curve is then least-square fitted by eq 1 to give the best fit "single" repopulation rate. This gives a single ground-state repopulation rate expected from eq 2 of $K = 1/1.8$ ns^{-1} for equal contributions of 1/3.3- and 1/1.1-ns^{-1} repopulation rates. Thus, our value of the ground-state recovery rate of $K = 1/(1.6 \pm 0.3)$ ns^{-1} is in good agreement with the measured TRP fluorescence decay results.

The un-ionized TYR residues in glucagon which give rise to the 1610-cm^{-1} band in Figure 8 show rapid ground-state recovery rates as shown in Figure 10. Within the statistics of the glucagon data we find that our ca. 4-ns pulse width allows us to determine that the ground-state recovery rate is faster than ca. 1/50 ps^{-1} for these TYR residues. No time-resolved measurements of TYR emission from glucagon have been reported. It is highly probable that these rapid TYR ground-state repopulation rates are dominated by energy transfer between the two TYR residues. The glucagon TYR residue pKa's of 9.9 and 10.6 suggest that at pH = 10 about 60% of the glucagon molecules have either TYR 10 or TYR 13 ionized, 30% have neither TYR residue in the ionized form, and 10% have both residues ionized.[21] Energy transfer between unionized TYR can occur as has been shown by polarization measurements. Although the process is not generally efficient due to the unfavorable overlap of TYR absorption and emission spectra, energy transfer between TYR residues has been shown to be significant in TYR–TYR and TYR–GLY–TYR peptides.[24] Depending on the specific conformations of glucagon, the close proximity of TYR 10 and TYR 13 could allow for energy transfer in the case where neither TYR is ionized. The remaining TYR residues are likely to be involved in TYR-to-tyrosinate energy transfer. The transfer of electronic excitation energy from TYR to tyrosinate is much more favorable due to the large red-shift in the tyrosinate absorption spectrum as discussed above. Edelhoch et al.[24] have shown that there is no detectable TYR fluorescence from half ionized peptides of the form TYR–$(GLY)_{0-2}$–TYR indicating complete energy transfer in each case. These results are consistent with our rapid TYR ground-state recovery rates and TYR 10–TYR 13 energy transfer in glucagon at pH 10.

Protein Photophysics in Higher Excited Singlet States. Our observations that ground-state recovery rates of TRP residues modeled by eq 2 generally agree with the fluorescence decay measurements of these residues has important implications. Our Raman saturation methodology study utilizes 225-nm excitation, in resonance with the B_b excited electronic state, while the fluorescence studies all utilize longer wavelength excitation in resonance with the L_a–L_b excited states. The agreement between these two relaxation rate measurements indicates that the TRP residue internal conversion efficiency is essentially 100% in the proteins we have studied and that the relaxation from fluorescing levels is dominated by direct repopulation of the ground state. The rapid ground-state repopulation rates for the TYR residues in Mb and glucagon also imply efficient internal conversion to fluorescing levels, followed by rapid nonradiative relaxations such as the energy-transfer processes discussed above.

TRP and TYR residue internal conversion efficiencies of ca. 100% from higher singlet states are surprising in view of the large

(34) Formoso, C.; Forster, L. S. *J. Biol. Chem.* **1975**, *250*, 3738.
(35) Cowgill, R. W. *Biochem. Biophys. Acta* **1967**, *140*, 37.
(36) Cowgill, R. W. *Biochem. Biophys. Acta* **1970**, *207*, 556.
(37) Kronman, M. J.; Holmes, L. G. *Photochem. Photobiol.* **1971**, *14*, 113.
(38) Saito, Y.; Tachibana, H.; Hayashi, H. *Photochem. Photobiol.* **1981**, *33*, 239.
(39) Boesch, C.; Bundi, A.; Oppliger, M.; Wuthrick, K. *Eur. J. Biochem.* **1978**, *91*, 209.
(40) Werner, T. C.; Forster, L. S. *Photochem. Photobiol.* **1979**, *29*, 905.
(41) Ross, J. B. A.; Rousslang, K. W.; Brand, L. *Biochemistry* **1981**, *20*, 4361.

Table I. Tryptophan and Tyrosine Raman Cross Sections at 225-nm Excitation for Amino Acids, Small Peptides, and Various Proteins

molecule	no. of TRP residues	no. of TYR residues	TRP residue Raman cross section[a]			TYR residue Raman cross section[a]
			760[c]	1015[c]	1555[c]	1601–1617[c]
NATRPAM/NATYRA 1:1 mixture	1	1	1.9	1.3	2.1	0.71
TRP–TYR dimer	1	1	1.4	1.0	1.2	0.70
glucagon	1	2	1.6	1.2	1.8	*b*
lysozyme	6	3	1.2	0.9	1.4	0.60
myoglobin	2	2	2.4	1.9	3.3	1.2
hemoglobin	6	12	2.2	2.3	3.1	1.2
azurin[d]	1	2	1.1	1.2	1.9	1.0

[a] Raman cross sections in units of b/sr-molecule. [b] Raman cross sections uncertain due to tyrosine–tyrosinate equilibrium. [c] Band, cm^{-1}. [d] Reference 48a.

decreases in the fluorescence quantum yields, due to extensive solvated electron formation observed for a number of TRP and TYR derivatives with excitation wavelengths shorter than 240 nm.[23] The electron ejection process competes with internal conversion to emitting levels in aqueous solutions to give TRP and TYR radical species which survive much longer than our ca. 4-nsec pulse width. In the TRP residue case, this would be reflected in our results by significant values of ϕ_{out} required for our K values to be consistent with the measured fluorescence decay rates. Our previous 225-nm saturation study, for example, found ϕ_{out} values of 0.80 and 0.55 for TRP and TRPAM (pH 5), respectively.[14] In the TYR residue case, ϕ_{out} values in eq 2 as small as 0.15, for example, with a defined value of $K = 1/50$ ps^{-1}, would result in decreases of ca. 15% in the measured I_{RR}/I_S values over the energy flux range plotted in Figure 10. Clearly this is not observed for the Mb and glucagon cases.

The mechanism of electron ejection from TRP and TYR higher excited singlet states in water is generally thought to involve the initial formation of a charge transfer to solvent state,[44-46] which must require water molecules to closely approach the aromatic ring. It may be that the protein matrix impedes the formation of the charge transfer to solvent state to the extent that the TRP and TYR residues are not as accessible to water as the TRP or TYR monomers. This is reasonable in the case of Mb and lysozyme but seems invalid in the case of glucagon in which the TRP and TYR residues must be considered "exposed" to solvent. It is also possible that specific functional groups on nearby residues might modulate electron ejection, as has been suggested for the much less efficient (less than ca. 2% quantum yield)[23] electron ejection process from indole fluorescing levels. We can say only that the proteins studied here do not in general facilitate electron ejection from TRP or TYR higher excited singlet states.

Quantitative TRP and TYR Cross Sections in Proteins. The study of the ground-state repopulation rates of TYR and TRP residues in proteins, in addition to providing an additional probe of interresidue interactions, also allows us to accurately determine intrinsic Raman cross sections which are not artificially decreased due to saturation artifacts. The fitted values of I_{RR}/I_S at zero pulse energy flux density combined with the use of an internal Raman intensity standard enable us to quantitatively compare the Raman cross sections of TRP and TYR residues between different proteins. Table I displays the TRP and TYR cross section data derived here for the TRP–TYR dimer, glucagon, myoglobin, and lysozyme, while Table II lists the ground-state repopulation rates as discussed above. Added to Table I is 225-nm cross-section data for hemoglobin and the blue copper protein azurin recently measured in our laboratory.[47,48a] The striking result is that both TRP and TYR residue cross sections can vary by a factor of 2 or more in different proteins in their native forms. The local environments of the chromophores must therefore modulate the Raman cross section. This modulation of Raman intensity can serve as an additional tool for studying chromophore environments provided the nature of the modulation is understood.

Table II. TYR and TRP Derivative Ground-State Repopulation Rates

chromophore	ground-state repopltn rate, $\phi_{out} = 0$ (eq 2) (ns^{-1})
NATRPRAM	1/2.9
TRPAM (pH 5)	1/3.5
TRPAM (pH 9)	1/7.1
NATYR (pH 5)	1/5.5
TRP–TYR (pH 5)	1/5.0
TRP–TYR (pH 9)	1/0.7
TRP–TYR (pH 5)	1/0.7
myoglobin, TRP	1/0.07
myoglobin, TYR	1/0.04
lysozyme, TRP	1/0.4
lysozyme, TYR	1/6.0
glucagon, TRP	1/1.6
glucagon, TYR	1/<0.05

Raman cross-section differences could result from significant absorption spectral shifts due, for example, to hydrogen-bonding interactions for the TRP and TYR residues. The occurrence of such absorption spectral shifts would be difficult to determine from typical protein absorption spectra. Examination of detailed TRP Raman excitation profiles[48b] indicates that 225 nm is near the excitation profile peak, and a shift of 5 nm or more would be required for a factor of 2 change in cross section. Similar considerations for TYR[48] also suggest an ca. 5-nm shift would be required in the TYR case. Such large absorption shifts between proteins are unlikely, particularly when required for several residues.

Changes in the absorption and Raman cross sections may also occur due to differences in refractive index around the TRP and TYR residues in the protein matrix. These refractive index differences have been described by Bullough,[20] for example, who showed that at least two effects occur which modulate the effective electric field which induces transitions in the chromophore. The first derives from the isotropic refractive index contribution which gives rise to the "local field" correction used to explain differences between gas- and condensed-phase Raman cross sections[50] as well as between Raman cross sections for scatterers in solvents with different refractive indices.[51-53] This will always lead to an

(42) Cockle, S. A.; Szabo, A. G. *Photochem. Photobiol.* **1981**, *34*, 23.
(43) Grinvald, A.; Steinberg, I. Z. *Biochem. Biophys. Acta* **1976**, *427*, 663.
(44) Steen, H. B.; Bowman, M. K.; Kevan, L. J. *J. Phys. Chem.* **1976**, *80*, 482.
(45) Zechner, J.; Kohler, G.; Getoff, N.; Tatischeff, I.; Klein, R. *J. Photochem.* **1978**, *9*, 304.
(46) Ottolenghi, M. *Chem. Phys. Lett.* **1971**, *12*, 339.
(47) Song, S.; Asher, S. A. Manuscript in preparation.
(48) (a) Sweeney, J. A.; Harmon, P. A.; Asher, S. A.; Hutnik, C. M.; Szabo, A. G. *J. Am. Chem. Soc.* Submitted for publication. (b) Sweeney, J. A.; Asher, S. A. *J. Phys. Chem.* **1990**, *94*, 4784.
(49) Ludwig, M.; Asher, S. A. *J. Am. Chem. Soc.* **1988**, *110*, 1005.
(50) Abe, N.; Wakayama, M.; Ito, M. *J. Raman Spectrosc.* **1977**, *6*, 38.
(51) Fini, G.; Mirone, P.; Pattella, P. *J. Mol. Spectrosc.* **1968**, *28*, 144.
(52) Nestor, J. R.; Lippencott, E. R. *J. Raman Spectrosc.* **1973**, *1*, 305.
(53) Eckhardt, G.; Wagner, W. J. *J. Mol. Spectrosc.* **1966**, *19*, 407.

increase in Raman cross section with an increase in the averaged refractive index of the local microenvironment. The second effect arises from anisotropic contributions and describes the hypochromism discussed above and developed in an exciton model by Tinoco and others.[18,19] Depending on relative orientations the second effect can give rise to hypo- or hyperchromic effects although only hypochromic effects have been documented to date.

None of the phenomena above describe all the protein data measured thus far. Since the average refractive index in a protein interior in the ultraviolet is larger than that of water, chromophores partially or fully buried inside proteins should display larger cross sections than exposed residues. This argument fails to describe all of the data in Table I. NATRPAM and NATYRA are models for exposed TRP and TYR side chains in a polypeptide. The single exposed TRP residue in glucagon does indeed have cross sections similar to NATRPAM. In myoglobin and hemoglobin, the TRP and TYR cross sections are both significantly larger than NATRPAM and NATRA, suggesting buried or partially buried residues. The single TRP residue in azurin, however, is known to be completely buried[7,8,54,55] and yet has a dramatically smaller cross section than myoglobin or hemoglobin. In lysozyme, the TRP mode cross sections averaged over six residues are considerably smaller than those of NATRPAM—an effect not easily explained by average refractive index values. These results point out the difficulties which will be encountered in trying to relate detailed environmental or conformational information to resonance Raman intensities alone.

It is hoped that the combination of ground-state repopulation information with quantitative Raman cross-section data may make the spectroscopic signatures of aromatic amino acid environments in proteins more informative. Our relationship that might be useful is that both hypochromism and fluorescence quenching generally require fairly close contact of donor and acceptor chromophores (except in the case of heme groups as aromatic amino acid energy acceptors). Therefore rapid ground-state recovery rates might be accompanied by hypochromism and decreased Raman cross sections. This was observed for the TRP–TYR dimer at neutral and basic pH. The reduced TRP cross sections in lysozyme might also derive from a similar interresidue hypochromic interaction, in this case possibly with the disulfide bridges which quench the fluorescence and result in the fairly rapid ground-state repopulation rates measured for these residues. In the lysozyme case this is consistent with the recent observations of Kauffman et al.[56] who observed increases of two or more in the TRP fluorescence intensity and Raman cross sections upon partial unfolding of porcine and bovine growth hormone, where fluorescence quenching by a nearby disulfide bridge in the native conformation has been suggested.[57]

Summary and Future Directions

We have shown that the UV resonance Raman saturation methodology can monitor interresidue excited-state quenching interactions of TRP and TYR residues in proteins with excitation at 225 nm. The TRP residue ground-state repopulation rates obtained by this method agree well with the excited-state relaxation rates obtained by time-resolved fluorescence techniques. This result suggests that internal conversion from higher excited singlet states of TRP side chains in proteins to the fluorescing levels are essentially 100% efficient. New information is obtained for TYR residue excited-state relaxation rates. The success of these relaxation studies suggests it should also be possible to similarly monitor phenylalanine as well as TYR residue electronic relaxation processes in proteins with excitation wavelengths between 190 and 200 nm. The TRP Raman cross sections are dramatically reduced in the 190–200-nm spectral region and will not interfere with PHE or TYR vibrational studies.[58] The 1000- and 831–853-cm^{-1} features of PHE and TYR, respectively, offer completely resolved vibrational modes for saturation analysis with no overlap of amide vibrations. Even with pulse widths of 4 ns, it is possible to monitor lifetimes on the order of 100 ps. Shorter pulse widths will allow faster processes to be probed as long as a sufficient pulse energy can be delivered to cause measurable ground-state depletion.

It should also be mentioned that the UV saturation methodology can potentially monitor residue-specific excited-state relaxation rates in proteins and peptides. Isotopic substitution and/or deuterium exchange techniques may enable vibrational modes of similar chromophores to be resolved, thereby allowing residue selective UV saturation analysis. Harada and co-workers, for example, have recently utilized stepwise deuteration to characterize each of the six TRP residues in lysozyme.[59]

The Raman saturation methodology also is unique as a relaxation probe since it reports directly on ground-state repopulation; nonradiative relaxation pathways may be examined. In the blue copper protein azurin, for example, the fluorescence from the single TRP residue is strongly quenched, the major lifetime component being ca. 100 ps^{-1}.[7,8] The fluorescence-quenching mechanism is not clear but has been suggested to be electron transfer from the TRP fluorescing states to the copper center. We have carried out a preliminary UV saturation study of the TRP residue and found that the ground-state repopulation rate is fast (ca. $1/<200$ ps^{-1}).[48a] This suggests that if the fluorescence quenching were due to electron transfer, then an additional mechanism is required where the TRP radical species formed is rapidly reduced back to ground-state TRP.

Conclusions

UVRR saturation spectroscopy will become an important technique for monitoring TRP, TYR, and PHE residue excited-state relaxation rates in proteins. This information coupled with quantitative UV Raman cross sections will advance the utilization of all three of these aromatic amino acid residues as unique probes of protein structure and dynamics.

Acknowledgment. We gratefully acknowledge support of this work from NIH Grant IR01GM30741-09. We thank Joyce Sweeney and Sunho Song for use of the azurin and hemoglobin TRP and TYR cross-section data in Table I.

(54) Finazzi-Argo, A.; Rotilio, G.; Avigliano, L.; Geurrieri, V. B.; Mondovi, B. *Biochemistry* **1970**, *9*, 2009.
(55) Szabo, A. G.; Stepanik, T. M.; Wayner, D. M.; Young, N. M. *Biophys. J.* **1983**, *41*, 233.
(56) Kauffman, E. W.; Thamann, T. J.; Havel, H. A. *J. Am. Chem. Soc.* **1989**, *111*, 5449.
(57) Parr, G. R.; Salsgiver, W. J.; Schilling, R. J.; Krivi, G. G.; Wood, D. C. Abstracts of Paper; FASEB, Las Vegas, NV, 1988; Abstract 8556.
(58) Fodor, P. A.; Copeland, R. A.; Grygon, C. A.; Spiro, T. G. *J. Am. Chem. Soc.* **1989**, *111*, 5509.
(59) Miura, T.; Takeuchi, H.; Harada, I. *Biochemistry* **1988**, *27*, 88.